

### Contents lists available at ScienceDirect

## International Journal of Pharmaceutics

iournal homepage: www.elsevier.com/locate/iipharm



# Induction of immunogenic cell death of cancer cells through nanoparticlemediated dual chemotherapy and photothermal therapy



Niloofar Heshmati Aghda<sup>a</sup>, Shahad M. Abdulsahib<sup>b</sup>, Carli Severson<sup>b</sup>, Emilio J. Lara<sup>b</sup>, Susana Torres Hurtado<sup>c</sup>, Tugba Yildiz<sup>a</sup>, Juan A. Castillo<sup>b</sup>, James W. Tunnell<sup>c</sup>, Tania Betancourta

- Materials Science, Engineering and Commercialization Program, Texas State University, San Marcos, TX, USA
   Department of Chemistry and Biochemistry, Texas State University, San Marcos, TX, USA
   Cpepartment of Biomedical Engineering, The University of Texas at Austin, Austin, TX, USA

#### ARTICLE INFO

Combination therapy
Damage associated molecular patterns
Immunogenic cell death Nanoparticles Photothermal therapy PLA-PEG

#### ABSTRACT

The use of nanomedicines to induce immunogenic cell death is a new strategy that aims to increase tumor immunogenicity and thereby prime tumors for further immunotherapies. In this study, we developed a nanoparticle formulation for combinatory chemotherapy and photothermal therapy based only on materials previously used in FDA-approved products and investigated the effect of the combinatory therapy on the growth inhibition and induction of immunogenic cell death in human MDA-MB-231 breast cancer cells. The formulation consists of  $\sim$ 108-nm nanoparticles made of poly(lactic acid)-b-methoxy poly(ethylene glycol) which carry doxorubicin for chemotherapy and indocyanine green for photothermal therapy. A 0.3 mg/mL suspension of NPs increased the medium temperature up to 10 °C upon irradiation with an 808-nm diode laser. In vitro studies showed that combination of laser assisted indocyanine green-mediated photothermal therapy and doxorubicin-mediated chemotherapy effectively eradicated cancer cells and resulted in the highest level of damage-associated molecular pattern presentation (calreticulin, high mobility group box 1, and adenosine triphosphate) compared to the individual treatments alone. These results demonstrate that our nanoparticle-mediated combinatory approach led to the most intense immunogenic cell death when compared to individual chemotherapy or photothermal therapy, making it a potent option for future *in vivo* studies in combination with cancer im munotherapies.

### 1. Introduction

New cancer cases in the United States are expected to increase to > 1 million per year for men and 900,000 cases per year for women by 2020 (Weir et al., 2015). Several cancer treatment methods in cluding chemotherapy, radiotherapy, hyperthermia and immunotherapy have been developed and have achieved a moderate degree of success. The major problems of all approaches are cancer recurrence and the high toxicity and side effects caused by high dosages of these treatments (Sharma and Allison, 2015). Rational combination of two or more methods can be considered as a solution which takes advantage of different mechanisms to kill cancer cells and decreases the probability of cancer recurrence (Moy and Tunnell, 2017). Furthermore, combined methods can work synergistically to improve the efficacy of treatment. In other words, less dosage of each treatment is required to induce the same therapeutic effect, leading to less side effects (Moy and Tunnell, 2017; Ott et al., 2017; Kourie and Klastersky,

Immunotherapy has gained successful outcomes in the treatment of metastatic cancers. However, low response rates and the potential for

Abbreviations: ATP, Adenosine Triphosphate; BSA, Bovine Serum Albumin; CRT, Calreticulin; DAMP, Damage Associated Molecular Patterns; DAPI, 4',6-diamidino-2-phenylindole; DL%, Drug Loading %; DLS, Dynamic Light Scattering; Dox, Doxorubicin; FBS, Fetal Bovine Serum; GPC, Gel Permeation Chromatography; HMGB1, High Mobility Group Box 1; ICD, Immunogenic Cell Death; ICG, Indocyanine Green; IR, Infrared; IALS, Low-Angle Light Scattering; mPEG, Methoxy-PEG; MTT, Thiazolyl Blue Tetrazolium Bromide Assay; NIR, Near Infrared; NP, Nanoparticle; NT, No Treatment; OH-PEG-OCH<sub>3</sub>, Heterofunctional poly(ethylene glycol) Methyl Ether; PBS, Phosphate Buffered Saline; PEG, Poly(ethylene glycol); PLA-mPEG, Poly(lactic acid)-b-methoxy poly(ethylene glycol); PS, Polystyrene; RALS, Right-Angle Light Scattering; ROP, Ring Opening Polymerization; SD, Standard Deviation; SEM, Scanning Electron Microscopy

\* Corresponding author at: Department of Chemistry and Biochemistry, Texas State University, 601 University Drive, San Marcos, TX 78666, USA.

E-mail address: tania.betanc ırt@txstate.edu (T. Betancourt).

Received 20 May 2020: Received in revised form 11 August 2020: Accepted 16 August 2020

Available online 06 September 2020 0378-5173/ © 2020 Elsevier B.V. All rights reserved.

high toxicity are the two main drawbacks of this treatment. The reason for low response rates is believed to be the nonimmunogenic environment of the tumor which contains numerous factors that help to evade immune system activation and attack (Sharma and Allison, 2015). However, the tumor microenvironment can be altered into an immunogenic one with a pre-treatment that induces immunogenic cell death (Sharma and Allison, 2015; Kroemer et al., 2013).

Immunogenic cell death (ICD) is a form of cell death that can induce an anti-tumor immune response by activation of dendritic cells, thereby initiating a cascade process leading to antigen-specific T-cell response (Kroemer et al., 2013). ICD is characterized by the secretion or surface presentation of damage-associated molecular patterns (DAMPs), including calreticulin (CRT), high mobility group box 1 (HMGB1), adenosine triphosphate (ATP) and heat shock proteins (Kroemer et al., 2013; Krysko et al., 2012).

Photothermal therapy (PTT) has been proposed as a method to induce ICD (Kroemer et al., 2013; Wang et al., 2014; Zhang 2019b). PTT is a treatment in which the tumor cells are killed through localized heat induced by laser treatment. Hyperthermia can result in direct cell damage, apoptosis induction, microvascular damage, altered cytokine expression, and alterations in immune response (Nikfarja et al., 2005). Immune response changes occur through activation of dendritic cells, delivery of tumor-specific agents to the lymph nodes, and activation of T cells specific to the tumor specific agents. A biocompatible material which can absorb near infrared (NIR) laser energy targeted to the tumor is required for PTT. Gold NPs, carbon-based nanostructures like graphene, carbon nanotubes, conductive polymerbased materials such as poly(ethylene dioxythiophene) nanoparticles (NPs) and dye encapsulated NPs have been previously used for this purpose (Wang et al., 2014; Yuan et al., 2013; Huang et al., 2006; Cantu et al., 2017). Amongst all, the only compound which has been approved by FDA for clinical use is the dye indocyanine green (ICG) (Drugs@FDA), which is currently used as a clinical imaging agent. ICG-containing NPs have been reported to be effective PTT agents in cancer research (Sheng et al., 2013).

Similarly, anticancer therapy with the chemotherapeutic agent Doxorubicin (Dox) has been proved to induce ICD, relieve tumoral immune suppression in the tumor environment and stimulate antitumor adaptive immunity (Zhang et al., 2019; Mattarollo et al., 2011; Bezu et al., 2015; Kersten et al., 2015; Galluzzi et al., 2017; Dudek et al., 2013; Casares et al., 2005). Dox shows cytotoxic activity by inhibiting DNA replication within cancer cells. However, its nonspecific action leads to severe side effects, especially in higher dosages (Yoo et al., 2000). Therefore, a combination of chemotherapy and PTT with moderate dosages is expected to provide an immunogenic microenvironment that is susceptible to immune response.

In this study, we report the preparation of NPs containing ICG and Dox –a chemotherapeutic agent which has been reported to induce ICD (Mattarollo et al., 2011)— through nanoprecipitation of poly(lactic acid)-b-methoxy poly(ethylene glycol) (PLA-mPEG), a polymer that is well known to be biodegradable and biocompatible (Xiao et al., 2010). These NPs were evaluated as agents for dual PTT and chemotherapy to eradicate cancer cells. In addition, our studies investigated the effectiveness of NP-mediated combination therapy at inducing ICD in vitro compared to chemotherapy and PTT alone through the evaluation of DAMP presentation by the treated cancer cells.

### 2. Materials and methods

#### 2.1. Material

Heterofunctional poly(ethylene glycol) methyl ether (OH-PEG-OCH<sub>3</sub>, Mn 5 kDa) and bovine serum albumin (BSA) were acquired from Sigma-Aldrich. Tin(II) 2-ethylhexanoate (stannous octoate, Sn(Oct)<sub>2</sub>), doxorubicin hydrochloride (Dox), and thiazolyl blue tetrazolium bromide (MTT) were obtained from Alfa Aesar (Ward Hill, MA). Indocyanine green (ICG) was obtained from MP Biomedicals (Irvine, CA). ATP Determination Kit was obtained from Invitrogen (Carlsbad, CA). Rabbit anti-calreticulin antibody (ab2907) and rabbit anti-HMGB1 antibody (ab79823) were purchased from Abcam (Cambridge, UK). Goat anti-rabbit IgG (H&L) DyLight 488 conjugate was obtained from ImmunoReagents, Inc. (Raleigh, NC). 4',6-Diamidine-2'-phenylindole (DAPI) dihydrochloride was purchased from EMD Millipore Corporation (Burlington, MA). 10x phosphate buffer saline (PBS) was received from SeraCare (Milford, MA). Ultrapure deionized water was obtained from a Millipore Direct Q system. All of the other solvents used were ACS grade.

### 2.2. Methods

### 2.2.1. Polymer synthesis

p,t-Lactide was dissolved in ethyl acetate at 70 °C and cooled down to room temperature to recrystallize. These unimers were freeze dried to remove any remaining solvent prior to use. PLA-mPEG was synthesized through ring opening copolymerization (ROP) of p,t-lactide with methoxy-PEG (mPEG) ( $M_{\rm w}=5000~{\rm g/mol})$  in toluene using stannous octoate (Sn(Oct)<sub>2</sub>) as a catalyst at 110 °C for 24 h under an Ar atmosphere, as shown in Fig. 1 (Yildiz et al., 2018). The product was then dissolved in acetone, and the copolymer was precipitated by adding cold ( $-86~{\rm ^{\circ}C})$  ethyl ether and separated through 10 min of 9798g centrifugation at 4 °C (Avanti J-26 XPI, Beckman Coulter, US). The purification process was repeated three times and the product was lyophilized and kept at  $-25~{\rm ^{\circ}C}$  for further use.

### 2.2.2. Polymer characterization

The copolymer was characterized by <sup>1</sup>H NMR spectroscopy using a Bruker Avance III 400 Hz spectrometer to confirm the copolymer synthesis and estimate the molecular weight. Molecular weight was also estimated using a Viskotek gel permeation chromatography (GPC) system with a Viskotek 270 dual detector (Right-Angle Light Scattering (RALS)) and Low-Angle Light Scattering (IALS). The estimated molecular weight was determined relative to polystyrene (PS) standards with molecular weights of 5,200, 13,000 and 30,000 g/mol prepared in HPLC-grade CHCla (5 mg/ml). The mobile phase was HPLC-grade chloroform with a flow rate of 1 mL/min. The samples were injected through a solvent delivery system (VE 1122) into a Malvern T3000 GPC column.

## 2.2.3. NP preparation

PLA-mPEG NPs were made through nanoprecipitation. Briefly, 100 µL of an organic phase containing PLA-mPEG (15 mg/mL), ICG (1 mg/mL) and Dox (1.6 mg/mL) in a mixture of acetone and DMSO (ratio 3:2) was added dropwise to 2 mL ultrapure water while stirring at

 $\textbf{Fig. 1.} \ \, \textbf{Ring opening copolymerization of poly(lactic acid)} \cdot \textbf{\textit{b}-poly(ethylene glycol) (PLA-mPEG) in the presence of } \textbf{Sn(Oct)}_2 \ \text{as a catalyst.} \\$ 

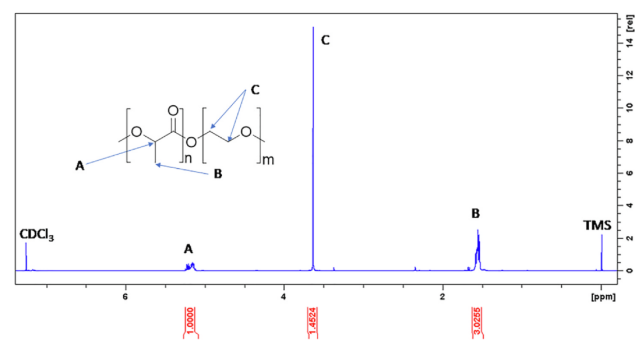


Fig. 2. NMR Spectrum of poly(lactic acid)-b-poly(ethylene glycol) dissolved in CDCl<sub>3</sub>

960 rpm. NPs were separated from unloaded Dox and ICG through one-hour centrifugation at 74,200g (Avanti J-26 XPI, Beckman Coulter, US). NPs were then resuspended in water and characterized. Blank NPs were made with the same method except that the organic phase did not contain ICG or Dox. For confirmation of reproducibility of NP preparation, independent NP batches were made and characterized over a period of several months.

## 2.2.4. NP characterization

NPs were characterized by dynamic light scattering (DLS) to measure their hydrodynamic size and electrophoretic light scattering to determine their zeta potential using a Malvern ZetaSizer Nano ZS instrument. For measurement of hydrodynamic size, NPs were suspended in water. Zeta potential measurements were carried out in 1 mM KCl. the stability of NPs in complete cell media (described below) at 37 °C was investigated by tracking NP size variation over a period of 72 h.

The morphology of dried NPs was investigated by scanning electron microscopy (SEM) using an FEI Helios NanoLab 400 microscope after coating them with a 2-nm layer of iridium by coating with an Electron Microscopy Sciences EMS150T ES sputter coater.

Drug loading (DL%) was calculated using Equation (1) in which the mass of loaded agents (ICG or Dox) was determined by UV–vis spectroscopy using a Biotek H4 multimode plate reader ( $\lambda_{\rm Abs}=476$  nm for Dox and  $\lambda_{\rm Abs}=798$  nm for ICG). The total mass of NPs was measured by scale after lyophilization.

$$DL\% = 100 \times \frac{Mass \ of \ agent \ in \ NPs}{Total \ mass \ of \ NPs}$$
 (1)

## 2.2.5. NP degradation

To investigate the degradability of the polymeric NPs, gel permeation chromatography was used to compare the polymer's molecular weight distribution before and after degradation. Blank NPs were made as described earlier, resuspended in phosphate buffered saline (PBS, pH 7.4) and incubated at 37  $^{\circ}$ C for 30 days. The suspension was then lyophilized and dissolved in HPLC grade chloroform. The resulting mixture was then filtered through Whatman filter paper, 0.2  $\mu$ m syringe filter and 20 nm syringe filter prior to analysis by GPC.

## 2.2.6. Agent release

The *in vitro* drug release behavior of the NPs was studied for 30 days. Release studies were performed by placing 150  $\mu$ L of 13.3 mg/mL suspension of the NPs (0.56 mg/mL Dox and 0.36 mg/mL log) in release buffer in a dialysis tube (D-Tube<sup>TM</sup> Dialyzer Mini, MWCO 6–8 kDa) and immersing these tubes in 4 mL of PBS solution (pH 7.4)

containing 5 mg/mL bovine serum albumin (BSA) at 37 °C. BSA was included in the release buffer to enhance the stability of ICG in aqueous environment and enable reliable measurement of the concentration of this agent. 100  $\,\mu$ L samples were taken from the 4-mL dialysate at predetermined time intervals to determine the concentration of ICG and Dox released by UV–Vis absorption spectroscopy. The volume of the dialysate was maintained through the study by immediately replacing the volume taken with fresh release buffer.

### 2.2.7. PTT conversion

NPs were irradiated by an 808-nm laser diode (RLCO-808-1000G, 9 mm; Roithner Lasertechnik GmbH, Wien, Austria) for 10 min at room temperature. An indium antimonide infrared (IR) camera (FLIR Systems, Inc., Wilsonville, OR, USA) was used to measure the temperature change of the samples. The samples were irradiated at an irradiance of 0.3 W/cm² (laser power = 84.8 mW, spot diameter = 6 mm). All of the measurements were conducted in 96-well plates with 100  $\mu L$  of sample. The concentration of NPs in suspension in complete cell media was 0.3 mg/mL and complete cell media (described below) was used as the control.

Utilizing the temperature elevation achieved over the time of irradiation of the NPs, the thermal dose utilized for *in vitro* studies was calculated in terms of the cumulative equivalent minutes at 43 °C (CEM43) (Dewhirst et al., 2003; Sapareto and Dewey, 1984) per Equation (2):

$$CEM43 = tR^{(43-T)}$$
 (2)

where t represents a time interval in minutes, T the average temperature for a given time interval, and R = 0.25 for T < 43  $^\circ\text{C}$  or R = 0.5 for T > 43  $^\circ\text{C}$  (Dewhirst et al., 2003; Lee et al., 2019; de Bruijne et al., 2010; Sweeney et al., 2018). CEM43 has been proposed as a normalized thermal dose parameter that could enable comparison between various heating regimes associated with photothermal therapy and other methods of hyperthermia.

## 2.2.8. Cell culture

Human mammary adenocarcinoma MDA-MB-231 cells were obtained from the American Type Culture Collection (ATCC) and cultured in complete cell media consisting of Dulbecco's Modified Eagle's Medium (DMEM) without phenol red (Gibco, MD, USA) supplemented with 10% heat inactivated fetal bovine serum (FBS, RMBIO), 1% penicillin/streptomycin (WWR) and 1% 4-(2-hydroxyethyl)-1-piper-azineethanesulfonic acid (HEPES, HyClone) in a humidified atmosphere containing 5%  $\rm CO_2$  and 95% air at 37  $^{\circ}\rm C$ .

Laser irradiation of cells was conducted inside a custom-made

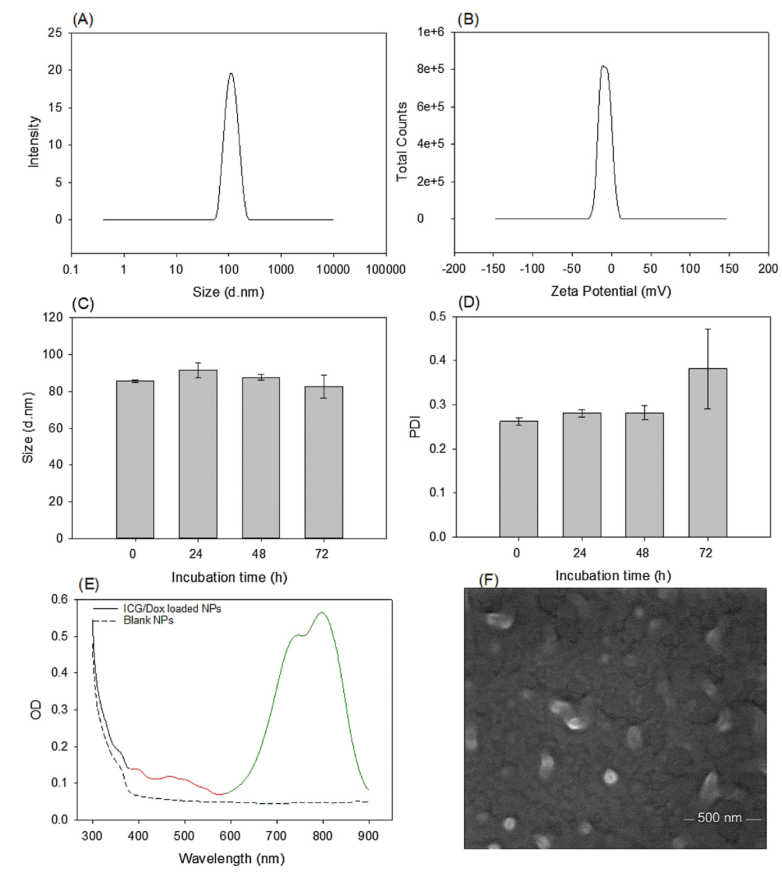


Fig. 3. NP characterization. (A) Size distribution of NPs by dynamic light scattering. (B) Zeta potential distribution of NPs. (C) Variation of NPs size and (D) PDI over 72 h incubation at 37 °C. Bars represent the means  $\pm$  5D (n = 3). No statistically significant differences were observed in the size or PDI of the NPs over time. (E) UV-Vis absorbance spectrum of NPs showing the presence of Dox (red) and ICG (Green). The spectrum of blank NPs (no Dox or ICG) at the same concentration is also shown for comparison. (F) SEM image of NPs.

incubator to simulate physiological temperature, as previously described (Nikfarjam et al., 2005). In this incubator, temperature was maintained at 37  $^{\circ}\mathrm{C}$  using filament bulbs wired to a STC-1000 probe temperature controller.

- 2.2.9. NP-mediated growth inhibition induced by chemotherapy and PTT Cells were seeded at a density of 5,000 cells/well in 96 well plates. 24 h later, when cells were attached to the wells, their media was replaced with the following treatments.
- (a) To study the effect of NP concentration, suspensions of NPs in complete cell media with concentrations ranging from 0.0 to 1.0 mg/mL were added to the cells. After 1.5 h incubation of cells with NPs at 37 °C, cells were treated with laser (0.3 W/cm², laser
- power = 118 mW, spot diameter = 7 mm) for 3 min.
- (b) To investigate the effect of laser irradiation time, the same procedure was followed, except that the concentration of NPs was set to 0.3 mg/mL and the irradiation time was varied from 0 to 9 min with a step size of 3 min.
- (c) To determine the effect of combination therapy, cells were treated with 0.3 mg/mL of NPs or with the equivalent concentration of free Dox in solution (12.7  $\mu$ g/mL = 23  $\mu$ M), free ICG in solution (8.1  $\mu$ g/mL = 10  $\mu$ M), or blank NPs (0.3  $\mu$ g/mL, no ICG or Dox). The equivalent concentration of Dox and ICG solutions were determined based on the drug loading percent for these agents within the NPs. The first group of the cells was irradiated with laser (0.3  $\mu$ g/m²) for 3  $\mu$ g/m after 1.5 h incubation at 37  $\mu$ g/m, while the second group was left without laser exposure.

4

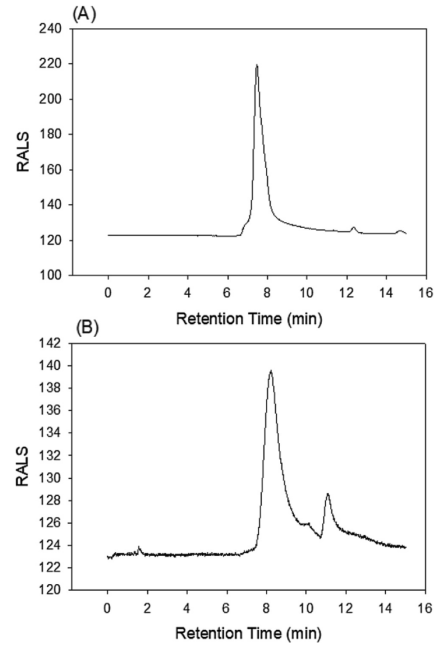


Fig. 4. GPC chromatograph of (A) intact polymer and (B) degraded polymer from NPs.

For all three studies, the MTT viability assay was performed after 48 h of incubation post laser irradiation at 37  $^{\circ}$ C. 10  $\mu$ L solution of 5 mg/mL MTT reagent in media was added to all the cells. Controls included cells that did not receive any treatment (NT) as well as cells that were treated with methanol for 15 min prior to viability assessment. After 2 h of incubation of the cells with the MTT reagent at 37  $^{\circ}$ C, the media was replaced with 200  $\mu$ L DMSO and plates were shaken for 15 min to allow proper dissolution of formazan crystals. The optical density of the solutions at 555 nm and 900 nm were measured with a Biotek 144 multimode plate reader.

## 2.2.10. Study of damage associated molecular patterns (DAMPs)

MDA-MB-231 cells were seeded in 96-well plates at a cell density of NPS (loaded with Dax and ICG) in media with a concentration of NPS (loaded with Dax and ICG) in media with a concentration of 0.3 mg/mL, or with a solution of free ICG or a solution of free Dax in media with equivalent concentration as in the NP suspension (23  $\mu$ M Dax or 10  $\mu$ M ICG). As a control, one group of cells was not treated (NT). Wells containing PTT agent (ICG or NPs) were irradiated with laser (0.3 W/cm²) for 3 min after 1.5 h incubation at 37 °C. Cells were returned to the incubator after laser treatment. After 30 min, 24 h, 48 h and 72 h, the level of DAMPs were determined as described below.

## (a) ATP release to extracellular fluid

The ATP Determination Kit (Invitrogen) was used to determine ATP release from the cells. The reagent was prepared per manufacturer recommendations and mixed with the cells' media (reagent: supernatant

volume ratio of 1:10). The luminescence of the solutions (peak at 560 nm) was then read with a Biotek H4 multimode plate reader using a 384-well plate.

### (b) Calreticulin determination

Immunocytofluorescence was used to determine the level of calreticulin (CRT) exposed on the cells' surface. Briefly, cells were fixed with 100  $\mu$ L 486 (t/v) formaldehyde for 20 min. Then, 100  $\mu$ L 88A (1% w/v) was added to block nonspecific absorption. BSA solution was discarded after 30 min, and the cells were incubated with 50  $\mu$ L rabbit polyclonal anti-CRT antibody (Abcam ab2907, 1:75 dilution in 0.1% w/v BSA) for one hour followed by one-hour incubation with 50  $\mu$ L of goat anti-rabbit 1gG DyLight 488 conjugate (1:1000 dilution in 0.1% w/v BSA) in the dark at room temperature. Cells were then incubated with 1  $\mu$ g/mL DAPI for 5 min with the purpose of staining cell nuclei for cell count. Multiple images were taken with an EVOS FL microscope and analyzed by ImageJ to determine the relative fluorescence and number of cells in each image. The relative fluorescence per cell was further calculated for each image.

### (c) HMGB1 release determination

HMGB1 release was determined indirectly by observing the extent of HMGB1 left within the cells via immunocytofluorescence. Briefly, cells were fixed with 4% v/v formaldehyde for 20 min, permeabilized with 0.2% v/v Triton X-100, blocked with 1% BSA for 30 min, incubated for one-hour with rabbit anti-HMGB1 antibody (Abcam ab79823, 1:250 dilution in 0.1% w/v BSA), and finally incubated for one hour with goat anti-rabbit IgG Dylight 488 conjugate (1:1000 dilution in 0.1% w/v BSA). Cells were then stained with 1 µg/mL DAPI and fluorescent images were taken and analyzed with the same method as for CRT.

## 2.2.11. Statistical analysis

The experiments were performed in at least triplicate (n  $\geq$  3) and the data was reported as the means  $\pm$  standard deviation (SD). One-way analysis of variance (ANOVA) with a post hoc Games-Howell multiple comparison was performed for identifying statistical differences between groups. The level of significance was set at  $^*p<0.05$ .

### 3. Results

### 3.1. Polymer preparation

The PLA-mPEG block copolymer was synthesized through ROP of p<sub>1</sub>L-lactide, as described in Fig. 1, and purified to separate unreacted p<sub>1</sub>L-lactide and PEG. Fig. 2 shows the <sup>1</sup>H NMR spectrum of the copolymer in D-chloroform. Peak A at 5.2 ppm belongs to methine proton and peak B at 1.6 ppm to the methyl protons (3 protons) of lactide. Peak C at 3.7 ppm is assigned to the 4 methylene protons in the PEG block (Yildiz et al., 2018; Du et al., 1995). The presence of both blocks in the copolymer confirms successful synthesis. Integration of each peak is proportional to the number of protons associated with them in the copolymer. Knowing the M<sub>w</sub> of mPEG (5000 g/mol), the M<sub>w</sub> of the copolymer was calculated to be 27,533 g/mol.

Molecular weight was also determined based on the data obtained from GPC by linear interpolation of the retention time of the polymer in the plot of  $\log(M_w)$  versus retention time obtained from PS standard samples. This method estimated the  $M_w$  to be 21,197 g/mol. The lower estimate in the  $M_w$  of the copolymer by GPC is a result of differences in its interaction with the mobile phase compared to that of the PS standards.

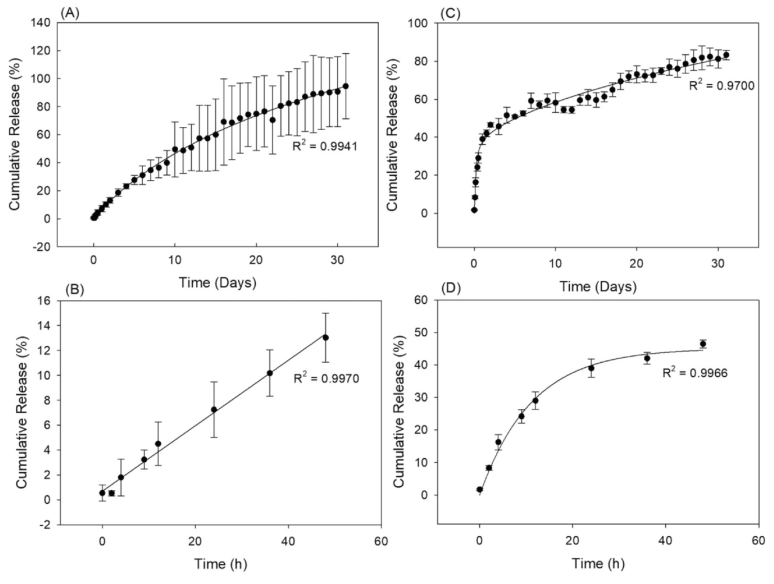


Fig. 5. (A) Release kinetics of ICG over 31 days and (B) 48 h. (C) Release kinetics of Dox over 31 days and (D) 48 h. Data points represent the means ± SD (n = 4).

### 3.2. Nanoparticle preparation

Nanoparticles were made through nanoprecipitation of PLA-mPEG block copolymer. In this method, a solution of the polymer in a mixture of acetone and DMSO, which dissolves both blocks of the copolymer very well, is added to an excess amount of water. The PLA block of the polymer is highly unstable in aqueous environment, leading to selfssembly of the polymer chains in the form of nanoparticles. Since the PEG block is hydrophilic, it acts as a stabilizer on the surface of the nanoparticles, preventing them from agglomerating and leading to the formation of nanoparticles with a core-shell structure (Gov 2000). In this study methoxy-PEG was chosen to make the NPs more stable. However, in future studies we will replace it with PEG-COOH which makes it possible to functionalize the NPs with targeting agents while maintaining other features equal (Yildiz et al., 2018; McCa et al., 2008; Özel et al., 2015). We adjusted the polymer molecular weight and polymer concentration in the organic solvent to make NPs with average size of 108.4 ± 2.1 nm. As Fig. 3.A shows, NPs had a narrow size distribution with a polydispersity index (PDI) of  $0.095 \pm 0.022$ . All the NPs were smaller than 200 nm, which means they can be good candidates for passive targeting based on the enhanced permeability and retention (EPR) effect (Joshi, 2014). The SEM image shown in Fig. 3.F confirms that the PLA/PEG block molecular weight ratio that we used leads to the formation of spherical NPs.

The distribution of zeta potentials of the NPs is shown in Fig. 3.B. The average of zeta potential was  $-7.73\pm1.17$  mV which causes electrostatic repulsion between NPs, thereby contributing to their stability in suspension (Honary and Zahir, 2013a, 2013b).

Fig. 3.C shows the size variation of NPs incubated in cell media at 37 °C for up to 72 h. No statistically significant change in the NPs size was observed in this time period, demonstrating that the NPs form a stable colloidal suspension even in the presence of proteins and salts.

Fig. 3.D shows that the PDI remains stable up to 72 h, at which point a slight increase in PDI is observed possibly due to the aggregation of some of the NPs; however, the values are not statistically different.

The hydrophobic core of the NPs makes it possible to load drugs

with hydrophobic regions through hydrophobic interactions. Harnessing this property of the NPs, we were able to load two amphiphilic therapeutic agents, ICG and Dox. The absorbance spectrum of the NPs shown in Fig. 3.E has a peak at 476 nm (red) and another at 798 nm (green) which confirms that Dox and ICG have both been successfully loaded within the NPs, respectively. The mass fraction of the therapeutic agents in the NPs was calculated to be 4.24 ± 0.17% for Dox and 2.69 ± 0.12% for ICG, which are both high enough to provide the required therapeutic effect without causing toxicity resulting from the need for a high dose of NPs (as later shown in Fig. 7.C). These weight percents were used to determine the concentrations of Dox and ICG to use as in cell studies. Other studies in which ICG and Dox have been coencapsulated within polymeric NPs have reported similar DL% and achieved reasonable therapeutic effects both in vitro and in vivo (Liu et al., 2019; Lozano et al., 2015; Xue et al., 2018; Yu et al., 2018). Combination therapy allows to utilize less concentration of each therapeutic agent, yet end with high antitumor effect due to the additive effect of the two treatment modalities. Moreover, the PTT effect can be increased by increasing the laser irradiation fluence.

## 3.3. NP degradation

The presence of ester bonds in PLA-mPEG leads to hydrolysis of the polymer in aqueous environments. Fig. 4 shows GPC chromatograph of the polymer before and after degradation over a period of 30 days. Since the NPs provide a high surface area which can be accessible for water molecules to hydrolyze the polymer, NPs are expected to undergo degradation within the 30 days that they were suspended in PBS. As

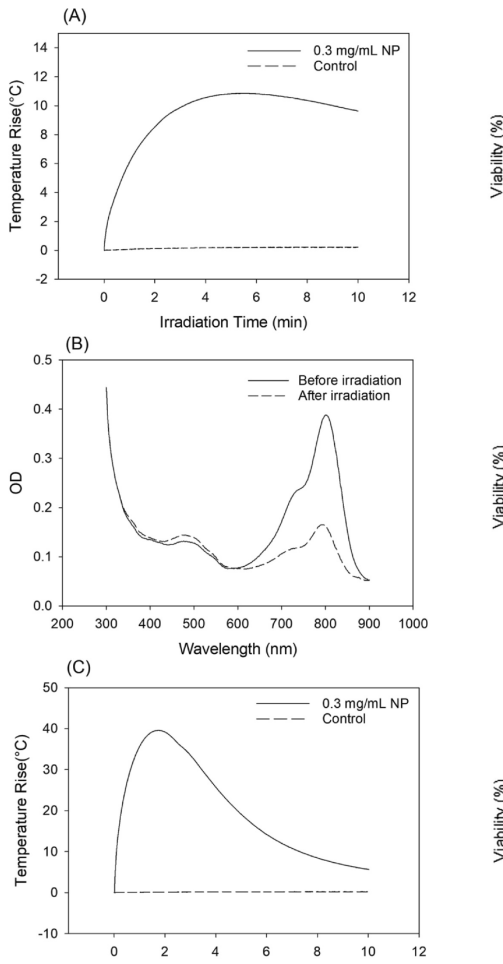


Fig. 6. (A) Temperature profile of NP suspension (0.3 mg/mL) in media irradiated with 808-nm diode laser at irradiance of 0.3 W/cm $^2$  for 10 min. (B) Absorbance spectrum of NPs before and after irradiation. (C) Temperature profile of NP suspension (0.3 mg/mL) in media irradiated with 808-nm laser at 3 W/cm $^2$  for 10 min.

Irradiation Time (min)

expected, the main elution peak shifted to a later elution time after degradation (from 7.5 to 8.3 min), the width of the peak broadened, and a second peak with a later elution time appeared, confirming that the polymer has undergone degradation and that its average molecular weight has been decreased due to chain cleavage. It should be noted, however, that degradation also leads to changes in the interaction of the polymer with the mobile and stationary phase of the GPC as a result

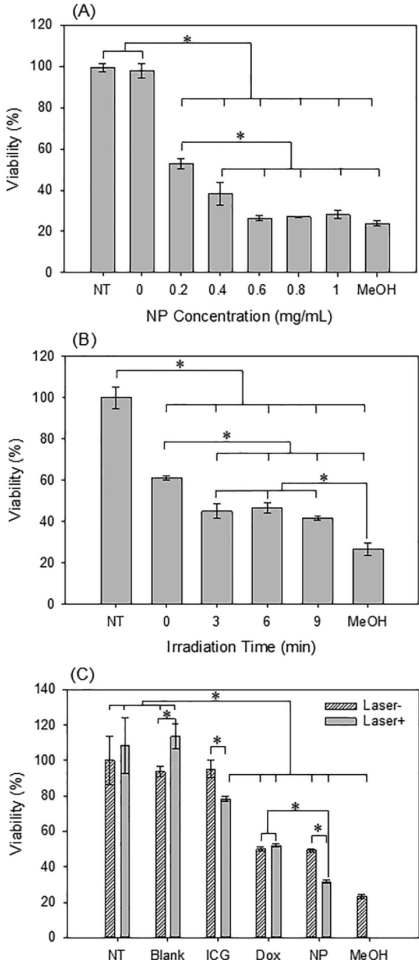


Fig. 7. Effect of NP treatment on cell viability. (A) Effect of NP concentration. Cells were irradiated with laser at 0.3 W/cm² for 3 min. No statistical difference was found between cells treated with 0.6, 0.8 or 1 mg/ml. of NPs and those treated with MeOH. (B) Effect of irradiation time on cell viability. Cells were exposed to 0.3 mg/ml. NPs and irradiated with laser at 0.3 W/cm² for varying time periods. No statistical difference was observed between cells treated with 3,6 or 9 min of laser irradiation. (C) Effect of each component of the NPs on cell viability. For all studies, cells were exposed to their respective treatment (blank NPs, ICG, Dox or NPs) for 48 h before their viability was assessed. Cells exposed to NPs or ICG were also irradiated with laser (0.3 W/cm²) 1.5 h after the beginning of the incubation with their respective treatment. NT = No treatment, MeOH = cells treated with methanol for 15 min, ns = no statistically significant difference. Bars represent the means  $\pm$  SD (n  $\geq$  3). \* Statistically significant difference (P < 0.05).

Treatment

7

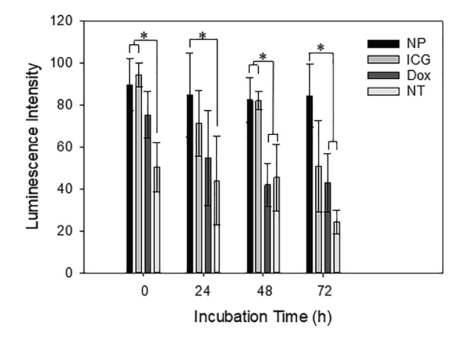


Fig. 8. Relative level of ATP release from the cells after treatment with NPs, ICG, or Dox, or with no treatment (NT) as a control. All the cells were incubated with their respective treatment 1.5 h prior to the laser irradiation. Incubation time in this figure represents the time that cells were incubated with the treatment after laser irradiation. \* Statistically significant difference (P < 0.05).

of the increasing contribution of functional groups of the degradation products (carboxylic acids and hydroxyl groups). Thus, accurate estimates of changes in polymer molecular weight are not feasible with the current protocol.

#### 3.4. Agent release

The release kinetics of both loaded agents, Dox and ICG, are shown in Fig. 5. As Fig. 5.A and B show, only 13% of ICG releases from the NPs in the first 48 h, leaving sufficient amount of ICG within the NPs to induce a PTT effect through laser irradiation. Similarly, approximately 50% of Dox releases within 48 h, and the rest of the Dox content releases gradually over 31 days. The best mathematical model which fitted the observed release kinetics was the Peppas-Sahlin equation (Ford et al., 1991; Peppas and Sahlin, 1989; Zhang et al., 2010) considering the lag time (Equation (3)) with R-squared values of 0.9941 and 0.9700 for ICG and Dox, respectively.

Released Fraction = 
$$k_1(t - T_{lag})^m + k_2(t - T_{lag})^{2m}$$
 (3)

Here k<sub>1</sub>, k<sub>2</sub> and m are constants. As the model describes, drug release from our NPs occurs through Fickian diffusion (first term) accompanied by polymer relaxation (second term) (Peppas and Sahlin, 1989).

### 3.5. PTT conversion

Fig. 6.A shows the temperature profile of 100 μL of suspension containing 0.3 mg/mL of NPs which is irradiated by laser at a 0.3 W/cm² irradiance for 10 min. As shown, the solution reaches its maximum temperature (~10 °C rise) after ~ 4 min. This temperature rise is high enough to eradicate tumor cells through hyperthermia (would reach > 43 °C starting from physiological temperature of 37 °C) (Herman et al., 1982). After this, the suspension starts cooling down due to the thermal instability of our photothermal agent, ICG, which, as the absorption spectrum in Fig. 6.B shows, decomposes after laser irradiation (Gathje et al., 1970), losing its ability to continue absorbing NIR light.

While most *in vitro* studies were conducted with NPs at a concentration of 0.3 mg/mL and laser irradiance at 0.3 W/cm², to demonstrate the dual effect of PTT and chemotherapy with low NP and thermal doses, it should be noted that the NPs can achieve a much higher temperature upon more intense laser irradiation. Fig. 6.C shows

the temperature profile for a suspension of NPs at 0.3 mg/mL irradiated at 3 W/cm $^2$  for 10 min. As shown, a temperature elevation of up to 40 °C can be readily achieved under these conditions.

### 3.6. Cell growth inhibition induced by NP-mediated chemotherapy and PTT

The effect of NP concentration and irradiation time on cell growth inhibition was determined. Fig. 7.4 shows the viability of cells treated with NPs at concentrations ranging from 0 to 1 mg/mL for 48 h and irradiated by laser at 0.3 W/cm² for 3 min. NPs at or exceeding 0.4–0.6 mg/mL in concentration cause a similar level of cell death to that observed in the cells that were killed by methanol exposure. A concentration of 0.3 mg/mL of NPs (between the 0.2 and 0.4 mg/mL tested) was selected for further tests. This selection was made in light of the fact that we aimed to demonstrate DAMP presentation by cells treated with the lowest possible NP dose. Too high a NP concentration and consequent high thermal dose would result in complete cell ablation that would prevent investigation of the presentation of these molecular markers in and from the cells.

Fig. 7.B shows the viability of cells treated with 0.3 mg/mL of NPs for 48 h and exposed to laser at 0.3 W/cm<sup>2</sup> for different time periods. Although irradiation by laser shows a lethal effect (higher viability is observed when exposure time is zero), increasing the exposure time from 3 min to 9 min does not result in any statistically significant difference in the viability of the cells. This observation is either due to the decomposition of ICG after laser irradiation as discussed in the previous section, leading to no further absorption of laser light after the maximum temperature is reached and thereby no further photothermal effect, or due to sufficient denaturation of proteins at the thermal dose received in these 3 min such that further heating does not cause added cell death. Further studies were then conducted with NPs at 0.3 mg/mL and with 3 min of laser irradiation. This thermal dose was then converted to CEM43 (Dewhirst et al., 2003; Sapareto and Dewey, 1984) as a way to enable comparison of the biological effect of our NPs compared to that induced by other hyperthermic treatments. In our case, PTT with 0.3 mg/mL of NPs irradiated for 3 min at 0.3 W/cm $^2$  equates to a CEM43 of 14.9 (logCEM43 of 1.17).

Fig. 7.C compares the lethal effect of NPs and each of their components. Cells which are treated with NPs are the least viable amongst all the treatments. The viability of the cells which are treated with the same concentration of blank NPs, both with and without laser exposure, are not significantly different from positive control with no treatment which confirms that the polymeric carrier is not toxic by itself. Cells that are treated with ICG solution, at the same concentration as in the NPs, but not irradiated are as viable as the positive control. However, their viability decreased when they were exposed to the laser beam which means PTT has still a significant effect at this low concentration. The same reduction in viability is observed when comparing the effect of NPs with and without irradiation. Cell viability reduction caused by Dox solutions at the same concentration as in the NPs did not further decrease upon laser exposure, as expected. NPs in the absence of irradiation also showed the same effect as Dox did. It should be noted that since the NPs or free drug were removed after 48 h of incubation, the cell growth inhibition observed upon treatment had to be caused by drug or NPs that had entered the cells in this time period. While about 50% of the drug would have been expected to release from the NPs in this time frame at a pH of 7.4, endocytosed NPs are typically exposed to acidic conditions that can lead to much faster degradation of the PLA polymer and, thereby, much faster drug release. In addition, once NPs are endocytosed, drug release can continue intracellularly even if the release kinetics were not affected. These two factors can explain why similar anti-cancer effect is seen in vitro for Dox solution and NPs. In conclusion, PTT and chemotherapy are responsible for approximately 20% and 50% of the viability decrease, respectively, while the carrier and the 808 nm laser do not decrease the viability of the cells by

8

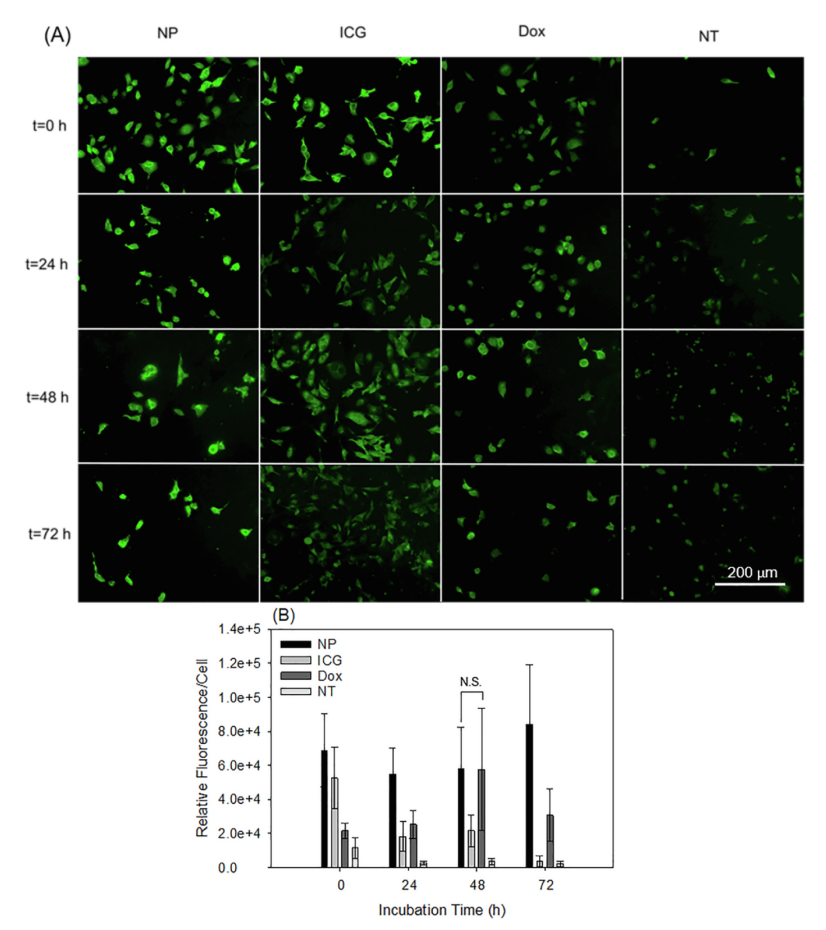


Fig. 9. (A) Representative images of fluorescent labeling of CRT exposed on the membranes after treatment over a 72-h incubation time period, and (B) their relative fluorescence measured by ImageJ software. Treatments include NP (combination therapy), ICG (PTT), Dox (chemotherapy) and no treatment (NT). Statistically significant differences were observed within treatments for a given incubation time or for a given treatment among the different incubation times, except where indicated as not statistically significant (N.S.).

## 3.7. ATP release

Cancer cells secrete ATP during ICD. Secreted ATP binds to dendritic cells through the P2XT and P2Y2 receptors leading to their maturation, which further induces an immune response against remaining tumor cells (Serrano-del Valle et al., 2019). Fig. 8 shows the release of ATP from the cells to the extracellular cell medium after treatment with NPs (with Dox, ICG and laser irradiation), ICG solution (with laser irradiation), or Dox solution after four different incubation times. In all of the four incubation times studied, the cells treated with NPs released significantly higher ATP to the extracellular medium compared to cells that received no treatment (NT). Another notable observation is that

although ICG-mediated PTT accounts for less cell death than treatment with Dox, as discussed in the previous section, it induces significantly higher ATP release than Dox does even after 48 h of incubation time, when the maximum effect of chemotherapy is expected. However, it should be noted that neither ICG nor Dox alone resulted in ATP release levels statistically different from NT at most time points.

## $3.8. \ \ Calreticulin \ (CRT) \ presentation$

Translocation of CRT to the cell surface occurs in ICD. CRT exposure leads to dendritic cell maturation through binding to the CD91 receptor (de Bruyn et al., 2015). Since two different treatment approaches with

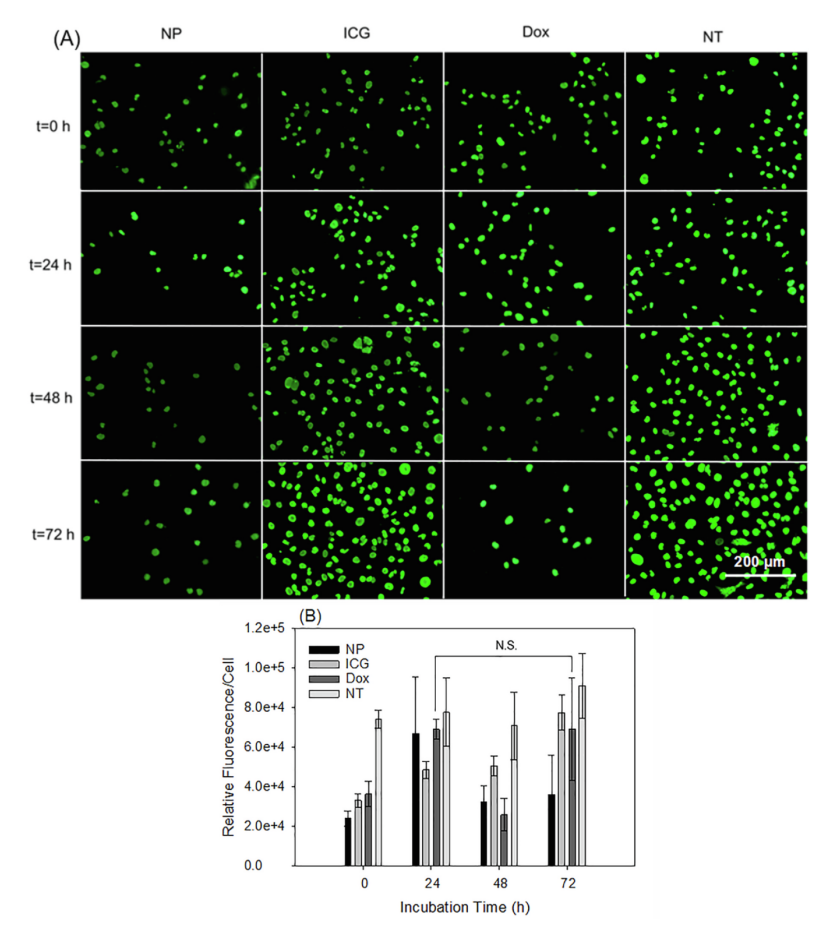


Fig. 10. Representative images of fluorescent labeling of HMGB1 remaining within the cells after treatment over a 72-h incubation time period, and (B) their relative fluorescence measured with ImageJ. Treatments include NP (combination therapy), ICG (PTT), Dox (chemotherapy) and no treatment (NT). Statistically significant differences were observed within treatments for a given incubation time or for a given treatment among the different incubation times, except where indicated as not statistically significant (N.S.).

different mechanism of action were used in this study, we traced CRT presentation on the cell membrane of the cells for 72 h to compare the effect of each treatment at each time point. Fig. 9.A shows one representative image of cells treated with ICG (PTT), Dox (chemotherapy) and NPs (combination therapy), along with a control group which did not receive any treatment. Fig. 9.B compares the relative fluorescence intensity per cell associated with surface CRT obtained from ImageJ for each treatment. The notable point in this figure is that NPs induced the highest level of CRT exposure at all the time points. PTT is the treatment that first imparts its effect. The reduction trend in CRT presentation observed over time for cells treated with ICG is due to the proliferation of the remaining cells which are not receiving further

treatment. However, the effect of Dox is observed after 48 h, as expected, preventing the combination therapy (NPs) from ceasing to induce presentation of this DAMP.

## 3.9. Release of HMGB1

HMGB1 is a nuclear protein that plays an important role in DNA transcription. Cells release HMGB1 from the nucleus to the cytoplasm and eventually to the extracellular medium during the process of ICD. Therefore, it is expected to observe a reduction in HMGB1 within the cells over time. Fig. 10.A shows one representative image of each treatment. As Fig. 10.B shows and as expected, the smallest amount of

HMGB1 left in the cells was observed upon combination therapy with NPs.

#### 4. Discussion

In this work we demonstrate the preparation of biocompatible biodegradable polymeric nanoparticles for dual chemotherapy and photothermal therapy using a simple nanoprecipitation process. The choice of a known polymer that has been previously utilized in FDAapproved formulations to enable dual photothermal/chemo-therapy was made specifically in light of the translational potential of the technology. The PLA-mPEG polymer utilized encapsulated Dox and ICG within the core-shell structure of the particles, providing them stability and controlling their release to the physiological environment. ICG was used as the PTT agent since it is a dye that is FDA-approved for bioimaging applications and has a long history of biocompatibility in humans (Drugs@FDA), making it an attractive agent for use in therapeutic applications. Dox was selected as the chemotherapeutic agent since it has been proven to relieve tumoral immune suppression and stimulate anti-tumor adaptive immunity (Mattarollo et al., 2011). The nano particles showed significant colloidal stability as a result of the PEG shell and negative zeta potential, and were able to maintain their size when suspended for up to 72 h in a physiologically relevant fluid.

In vitro studies demonstrated the ability of the NPs to locally increase the temperature from physiological temperature to over 43 °C upon irradiation with a NIR laser, which is a sufficient increase to lead to cell death (Huang et al., 2006). NIR light (~650–950 nm) can penetrate through tissues as deep as a few cm since tissue chromophores present minimal absorption and scattering in this range (Smith et al., 2009; Hudson et al., 2013), thereby making activation of these NPs suitable for the treatment of tumors that are superficial or that can be accessed endoscopically or laparoscopically.

Numerous groups, including our own, have utilized nanomedicines over the past decade for the treatment of primary tumors via chemotherapy or photothermal therapy (Cantu et al., 2017; Yildiz et al., 2018; Wei et al., 2019). In our current work, studies with cultured breast cancer cells demonstrated the ability of the dual treatment to induce a potent anti-cancer effect that resulted from the additive effect of chemotherapy and photothermal treatment. Other groups have also documented the additive effect of ICG-enabled PTT and chemotherapy on cancer cell eradication in the absence of a nanocarrier (Tang and on, 2009), and the synergy of nanoparticle-mediated chemotherapy and photothermal therapy on cancer treatment (Pacardo et al., 2015; Srinivasan et al., 2014). Only recently, however, has the use of these nanomedicines for modulation of systemic immunity against cancer been considered. The effect of localized hyperthermia induced via optical or magnetic stimulation of NPs on immune modulation has been studied by a few groups (Sweeney et al., 2018; Ito et al., 2013, 2003; Toraya-Brown and Fiering, 2014; Chen et al., 2016; Bear et al., 2013; Toraya-Brown et al., 2016). Similarly, the ability of certain chemotherapies to induce ICD is known (Bezu et al., 2015; Kersten et al., 2015; Galluzzi et al., 2017) and the combination of systemic chemotherapy and ICP has been the focus of recent clinical trials. Recently, Wen et al. demonstrated the induction of ICD by integration of palladium NPs as PTT agents and Dox as a chemotherapeutic agent into triglycerol monostearates (Wen et al., 2019). Nonetheless, the work herein reported is one of the first studies to investigate the effect of polymeric nanoparticle-mediated chemotherapy and photothermal therapy utilizing only materials previously utilized in FDAapproved systems in the induction of ICD. In addition, the thermal dose achieved with our NPs (1.17 log CEM43) is, as expected, lower than the "thermal window of ICD" reported by Sweeney et al. (2018) (3.3–5.6 log CEM43) for optimal PTT-mediated ICD induction and long-term survival in animal studies as a result of the additive effect from combination PTT and chemotherapy.

Our results demonstrate that codelivery of Dox and ICG in the NPs

and consequent dual treatment leads to the highest level of cancer cell death and highest extent of CRT presentation, HMGB1 release and ATP release. As such, this combinatorial therapy could potentially act in synergy with cancer immunotherapies that aim to make use of the patient's immune system to target tumor cells for elimination. Effective recognition and attack of cancer cells by killer T cells requires uptake, processing and presentation of tumor-specific antigens (immunogenic aberrant proteins produced by genetic mutations of cancer cells) by dendritic cells to native T cells (Cassetta and Kitamura, 2018). Unfortunately, poorly immunogenic tumors fail to initiate the immunogenic cascade. Our work demonstrates that dual chemotherapy and photothermal therapy induced by our NPs leads to ICD which is characterized by the release of tumor specific antigens and the DAMPs CRT, ATP and HMGB1. Importantly, our results show that the best response is obtained when the combination treatment utilizing NP-assisted chemotherapy and photothermal therapy is utilized. Future work will investigate if ICD mediated with these NPs could generate an antigen-specific immune response in vivo.

### 5. Conclusion

The PLA-mPEG NPs prepared in this study were confirmed to be cytocompatible, yet effective agents for dual photothermal therapy and chemotherapy. The NPs exhibited optimal size in the range of  $\sim \! 100$  nm and encapsulated sufficient Dox and ICG to mediate a therapeutic effect. This formulation showed promising results since a very low dose of NPs (0.3 mg/mL) and short laser irradiation time of 3 min led to an effective anti-cancer effect in MDA-MB-231 human breast cancer cells due to the additive therapeutic effect of each agent. Our investigation of DAMP presentation after treatment confirmed that the cells undergo ICD in response to our NP-mediated combinatorial treatment approach. Specifically, immunocytochemistry studies demonstrated that cells treated with NP-mediated dual therapy exhibited the highest level of presentation of CRT on the cell surface, as well as the highest release of HMGB1 and ATP compared to Dox-mediated chemotherapy or laser assisted ICG-mediated photothermal therapy alone. Thus, this treatment method is expected to be able to modulate the immunogenicity of tumor microenvironment which is believed to be the reason for the low response rate of currently available cancer immunotherapies.

### Funding

This work was funded in part by the Partnership for Research and Education in Materials (PREM) (NSF award DMR-1205670), the Chemistry REU on Molecular Innovation and Entrepreneurship (NSF award 1757843, funding to C.S.), the U.S. Department of Education HSI STEM Program (941.031c, award # P021C160036, funding to S.A.), the Texas State University Undergraduate Research Fellowship (funding to J.C.), and The University of Texas System and Mexico's Consejo Nacional de Ciencia y Tecnología (CONACYT) through the ConTex Postdoctoral Fellowships Program (funding to S.T.H.).

## CRediT authorship contribution statement

Niloofar Heshmati Aghda: Data curation, Formal analysis, Investigation, Methodology, Project administration, Writing - original draft. Shahad M. Abdulsahib: Data curation. Carli Severson: Data curation. Emilio J. Lara: Data curation. Susana Torres Hurtado: Data curation, Writing - review & editing. Tugba Yildiz: Data curation. Juan A. Castillo: Data curation. James W. Tunnell: Conceptualization, Formal analysis, Funding acquisition, Investigation, Methodology. Tania Betancourt: Conceptualization, Formal analysis, Funding acquisition, Investigation, Methodology. Project administration.

### **Declaration of Competing Interest**

The authors declare that they have no known competing financial interests or personal relationships that could have appeared to influence the work reported in this paper.

- Bear, A.S., Kennedy, L.C., Young, J.K., Perna, S.K., Almeida, J.P.M., Lin, A.Y., Eckels, P.C., Drezek, R.A., Foster, A.E., 2013. Elimination of metastatic melanoma using gold ermal therapy and adoptive T cell transfer. PLoS ONE 8 nanoshell-enabled photo (7), e69073.
- Bezu, L., Gomes-de-Silva, L.C., Dewitte, H., Breckpot, K., Fucikova, J., Spisek, R., Galluzzi L., Kepp, O., Kroemer, G., 2015. Combinatorial strategies for the induction of im-
- Bezul, L., Comes-ed-R., Kremer, G., Dewitte, K., Breckpot, K., Pucikova, J., Spöse, R., Galluzz, L., Kepp, O., Kremer, G., 2015. Combinatorial strategies for the induction of immonogenic call death. Front. Immon. 6, 187.
  Cantu, T., Walsh, K., Pattani, V.P., Moy, A.J., Tunnell, J.W., Irvin, J.A., Betancourt, T., 2017. Conductive polymer-based annoparticles for laser-mediated photothermal at lation of cancer synthesis, characterization, and in vitro evaluation. Int. J. Nanome 12 615
- 14, 615.

  Requires, N., Pequignot, M.O., Tesniere, A., Ghiringhelli, F., Roux, S., Chaput, N., Schmitt, E., Hamai, A., Hervas-Stubbs, S., Obeid, M., 2005. Caspase-dependent immunogenicity of doxorubicin-induced tumor cell death. J. Exp. Med. 202 (12), 1691–1701.
- 1691–1701.
  Cassetta, L., Kitamura, T., 2018. Macrophage targeting: opening new possibilities for cancer immunotherapy. Immunology 155 (3), 285–293.
  Chen, Q., Xu, L., Liang, C., Wang, C., Peng, R., Liu, Z., 2016. Photothermal therapy with immune-adjuvant nanoparticles together with checkpoint blockade for effective cancer immunotherapy. Nat. Commun. 7, 13193.
  de Bruijne, M., Van der Holt, B., van Rhoon, G.C., van der Zee, J., 2010. Evaluation of CEM43° CT90 thermal dose in superficial hyperthermia. Strahlenther. Onkol. 186 (8), 436–443.
- 436-443. ruyn, M., Wiersma, V.R., Helfrich, W., Eggleton, P., Bremer, E., 2015. The expanding immunomodulatory role of calreticulin in cancer immunity. Fron

- de Bruyn, M., Wiersma, V.R., Helfrich, W., Eggleton, P., Bremer, E., 2015. The evereexpanding immunomodulatory role of calreticulin in cancer immunity. Front. Oncol.
  5, 35.

  Bewhirst, M.W., Viglianti, B., Lora-Michiels, M., Hanson, M., Hoopes, P., 2003. Basic
  principles of themal dosimetry and thermal thresholds for tissue damage from hyperthermia. Int. J. Hyperth. 19 (3), 267–2974.

  Purgs@FDA: FDA Approved Drug Products. https://dow.uccessdata.fda.gov/scripts/
  cder/daf/index.cmir/event=overview.process&applno=011525.

  Du, Y.J., Lemstra, P.J., Nijenhuis, A.J., Van Aert, H.A., Bastiaansen, C., 1995. ABA type
  copolymers of lactide with poly (ethyleng elytool. Kinetic, mechanistic, and model
  studies. Macromolecules 28 (7), 2124–2132.

  Dudek, A.M., Garg, A.D., Krysko, D.V., De Ruysscher, D., Agostinis, P., 2013. Inducers of
  immunogenic cancer cell death. Cytokine Growth Factor Rev. 24 (4), 319–333.

  Ford, J.J., Mitchell, K., Rowe, P., Armstrong, D.J., Elliott, P.N., Rostron, C., Hogan, J.E.,
  1991. Mathematical modelling of drug release from hydroxypropylmethylcellulose
  matrices: effect of temperature. Int. J. Pharm. 71 (1–2), 95–104.

  Galluzzi, I., Buque, A., Kepp, O., Zitroegel, I., Kroemer, G., 2017. Immunogenic cell death
  in cancer and infectious disease. Nat. Rev. Immunol. 17 (2), 97–111.

  Gathje, J., Steuer, R.R., Nicholes, K., 1970. Stability studies on indocyanine green dye. J.
  Appl. Physiol. 29 (2), 1811–185.

  Govender, T., Riley, T., Ehtezazi, T., Garnett, M.C., Stolnik, S., Illum, L., Davis, S.S., 2000.

  Defining the drug incorporation properties of PLA-PEG nanoparticles. Int. J. Pharm.
  199 (1), 95–110.

  Honany, S., Zabit, F., 2013a. Effect of zeta potential on the properties of nano-drug delivery systems-a review (Part 1). Trop. J. Pharm. Res. 12 (2), 255–264.

  Honasy, S., Zabit, F., 2013b. Effect of zeta potential on the properties of nano-drug delivery systems-a review (Part 1). Trop. J. Pharm. Res. 12 (2), 255–264.

  Honasy, S., Zabit, F., 2013b. Effect of zeta potential on the properties of na

- infiltrating lymphocytes after hyperthermia using functionalized magnetite nano-particles. Nanomedicine 8 (6), 891–902.

  Joshi, M., 2014. Opportunities, challenges and pathways of nano-medicines: a concise review. J. Nanomed. Res. 1 (2), 00013.

  Kersten, K., Salvagno, C., de Visser, K.E., 2015. Exploiting the immunomodulatory properties of chemotherapeutic drugs to improve the success of cancer im-munotherapy. Front. Immunol. 6, 516.

  Kourie, H.R., Klastersky, J.A., 2016. Side-effects of checkpoint inhibitor-based combina-tion therapy. Curr. Opin. Oncol. 28 (4), 306–313.

  Kroemer, G., Galluzzi, L., Kepp, O., Zitvogel, L., 2013. Immunogenic cell death in cancer

- therapy, Annu. Rev. Immunol. 31, 51–72.

  yako, D.V., Garg, A.D., Kaczmarek, A., Krysko, O., Agostinis, P., Vandenabeele, P.,
  2012. Immunogenic cell death and DAMPs in cancer therapy. Nat. Rev. Cancer 12

  (12), 864–875.

  e, S.-T., Saigeti, G.P., Szasz, A.M., 2019. Oncological hyperthermia: The correct dosing in clinical applications. Int. J. Oncol. 54 (2), 627–643.

  n. Kuerong, Wang, Cheng, Ma, Huisong, Yu, Fangying, Hu, Fuqiang, Yuan, Hong, 2019.
  Water-responsive hybrid nanoparticles codelivering ICG and DOX effectively treat breast cancer via hyperthermia-aided DOX functionality and drug penetration. Adv. Healthcare Matter, 5 (8), 1801486.

  kanno, Neus, Al-Ahmady, Zahrna S., Beziere, Nicolas S., Ntziachristos, Vasilis, Kostarelos, Kostas, 2015. Monoclonal antibody-targeted PECylated liposome-ICG encapsulating doxorubicin as a potential theranostic agent. Int. J. Pharmaceut. 482 (1–2), 2–10.

- Kostarelos, Kostas, 2015. Monoctonal antibody-targeted PRG/yated liposome-ICG encapsulating dosorubicin as a potential theranostic agent. Int. J. Pharmaceut. 482 (1–2), 2–10.
   Mattarollo, S.R., Loi, S., Duret, H., Ma, Y., Zitvogel, L., Smyth, M.J., 2011. Pivotal role of innate and adaptive immunity in anthracycline chemotherapy of established tumors. Cancer Res. 71 (14), 4809-4820.
   McCarron, P.A., Marouf, W.M., Donnelly, R.F., Scott, C., 2008. Enhanced surface attachment of protein-type targeting ligands to poly (lactide-co-glycolide) nanoparticles using variable expression of polymeric acid functionality. J. Biomed. Mater. Res. Part A: Offic. J. Soc. Biomater. Jpn. Soc. Biomater. Australian Soc. Biomater. Res. Part A: Offic. J. Soc. Biomater. Jpn. Soc. Biomater. Australian Soc. Biomater. Korean Soc. Bioma. 87 (4), 873-884.
   Moy, A.J., Tunnell, J.W., 2017. Combinatorial immunotherapy and nanoparticle mediated hyperthermia. Adv. Drug Deliv. Rev. 114, 175-183.
   Nikfarjam, M., Muralidharan, V., Christophi, C., 2005. Mechanisms of focal heat destruction of liver tumors. J. Surg. Res. 127 (22), 208-223.
   Ott, P.A., Hodi, F.S., Kaufman, H.L., Wigginton, J.M., Wolchok, J.D., 2017. Combination immunotherapy: a road map. J. Immunoffire. Cancer 5 (1), 16.
   Ozel, T., White, S., Neuyen, E., Moy, A., Brenes, N., Choi, B., Betancourt, T., 2015.
   Pacardo, D.B., Neuyane, B., Rikard, S.M., Lu, Y., Mo, R., Mishra, R., Tracy, J.B., Wang, G., Ligler, F.S., Gu, Z., 2015. A dual wavelength-activatible gold nanorod complex for synergistic cancer treatment. Nanoscale 7, 12096.
   Peppas, N.A., Sahlin, J.J., 1989. A simple equation for the description of solute release. III. Coupling of diffusion and relaxation. Int. J. Pharm. 57 (2), 169-172.
   Sapareto, S.A., Dewey, W.C., 1984. Thermal dose determination in cancer therapy. Int. J. Rapareto, S.A., Dewey, W.C., 1984. Thermal dose determination in cancer therapy. Int. J

- arma, P., Allison (6230), 56–61.

- (6230), 56-61.
  Sheng, Z., Hu, D., Xue, M., He, M., Gong, P., Cai, L., 2013. Indocyanine green nanoparticles for theranostic applications. Nano-Micro Lett. 5 (3), 145-150.
  Smith, A.M., Mancini, M.C., Nie, S., 2009. Bioimagings second window for in vivo imaging. Nat. Nanotechnol. 4 (11), 710.
  Srinivasan, S., Manchanda, R., Lei, T., Nagesetti, A., Fernandez-Fernandez, A., McGoron, A. I. 2014. Targented prapagaticles for giventaneous deligency of champed parapagits.
- INVASIAI, S., MARICIARIOLA, R., LEI, I., PARGESCHI, R., PERIMIDEZ-PERIMINEZ, A., MICCOTOII, A.J., 2014. Targeted nanoparticles for simultaneous delivery of chemotherapeutic and hyperthermia agents-an in vitro study. J. Photochem. Photobiol., B 136, 81–90. eeney, E.E., Cano-Mejia, J., Fernandes, R., 2018. Photothermal therapy generates a thermal window of immunogenic cell death in neuroblastoma. Small 14 (20).
- 1800678.
  Tang, Y., McGoron, A.J., 2009. Combined effects of laser-ICG photothers herapy on ovarian cancer cells. J. Photochem. Photobiol., B 97 (3), 138-144.
- Toraya-Brown, S., Fiering, S., 2014. Local tumour hyperthermia as immunotherapy for
- Toraya-Brown, S., Fiering, S., 2014. Local tumour hypertnermia as immunotherapy to metastatic cancer. Int. J. Hyperth. 20 (8), 531–593.
  Toraya-Brown, S., Sheen, M.R., Zhang, P., Chen, L., Baird, J.R., Demidenko, E., Turk, M.J., Hoopes, P.J., Conejo-Garcia, J.R., Fiering, S., 2016. Local hyperthermia trea ment of tumors induces CD8+ T cell-mediated resistance against distal and sec-ondary tumors. In: World Scientificipp. 309–347.
  Wang, C., Xu, L., Liang, C., Kilang, J., Peng, R., Liu, Z., 2014. Immunological response triggered by photothermal therapy with carbon nanotubes in combination with an CTB 44 theoret to inhibit tensor, naturative Adv. Marcs 26 (49) 2115-418.
- triggered by photothermal therapy with caroon flanounces in community with an CTLA-4 therapy to inhibit cancer metastasis. Adv. Mater. 26 (48), 8154–8162.
  Wei, W., Zhang, X., Zhang, S., Wei, G., Su, Z., 2019. Biocompatible and bioactive engineered nanomaterials for targeted tumor photothermal therapy: a review. Mater
- gineered nanomateurs of the state of the sta sent, and future of cancer incidence in the United States: 1975 through 2020. Cat 121 (11), 1827–1837.

  Wen, Y., Chen, X., Zhu, X., Gong, Y., Yuan, G., Qin, X., Liu, J., 2019. Photothermal-themothermy integrated nanonarticles with transport.
- chemotherapy integrated nanoparticles with tumor microenvironment response hanced the induction of immunogenic cell death for colorectal cancer efficient treatment. ACS Appl. Mater. Interfaces 11 (46), 43393–43408.
- Xiao, R.Z., Zeng, Z.W., Zhou, G.L., Wang, J.J., Li, F.Z., Wang, A.M., 2010. Rev vances in PEG-PLA block copolymer nanoparticles. Int. J. Nanomed. 5, 10
- inces in Feb-Fix block Copolymer hambparticles. Inc. 3. Nationical. 3, 1037.
  iliao, Fang, Ting, Yin, Luyao, Jiang, Jianqi, He, Yunpeng, Dai, Yinghui, Wang, ongkai, 2018. Multistage delivery of CDs-DOX/ICG-loaded liposome for highly enetration and effective chemo-photothermal combination therapy. Drug Deliv. 25 Xue. Xiao. F (1), 1826–1839.
- t, T., Gu, R., Zauscher, S., Betancourt, T., 2018. Doxorubicin-loaded protease-acti-
- vated near-infrared fluorescent poymers and cancer. Int. J. Nanomed. 13, 961;
  Yoo, H.S., Lee, K.H., Oh, J.E., Park, T.G., 2000. In vitro and in vivo anti-tumor activities
  And Advorubicin-PLGA conjugates. J. Control. Release 68 (3),

- Yu, Lixia, Dong, Anjie, Guo, Ruiwei, Yang, Muyang, Deng, Liandong, Zhang, Jianhua, 2018. DOX/IGG coencapsulated liposome-coated thermosensitive nanogels for NIR-triggered simultaneous drug release and photothermal effect. ACS Biomater. Sci. Eng. 4 (7), 2424–2434.

  Yuan, A., Wu, J., Tang, X., Zhao, L., Xu, F., Hu, Y., 2013. Application of near-infrared dyes for tumor imaging, photothermal, and photodynamic therapies. J. Pharm. Sci. 102 (1), 6–28.

  Zhang, Y., Huo, M., Zhou, J., Zou, A., Li, W., Yao, C., Xie, S., 2010. DDSolver: an add-in

- program for modeling and comparison of drug dissolution profiles. AAPS J. 12 (3), 263–271.

  Zhang, D., Zhang, J., Li, Q., Song, A., Li, Z., Luan, Y., 2019b. Cold to hot: rational design of a minimalist multifunctional photo-immunotherapy nanoplatform toward boosting immunotherapy capability. ACS Appl. Mater. Interfaces 11 (36), 32633–32646.

  Zhang, J., Zhang, D., Li, Q., Jiang, Y., Song, A., Li, Z., Luan, Y., 2019a. Task-specific design of immune-augmented nanoplatform to enable high-efficiency tumor immunotherapy. ACS Appl. Mater. Interfaces 11 (46), 42904–42916.